Uptake and Cellular Effects of Polymethylmethacrylate on Human Cell Lines

Arthur Braun and Harald Seitz *

Posted Date: 29 November 2023

doi: 10.20944/preprints202311.1844.v1

Keywords: CREB; PMMA; micro-plastics; confocal microscopy; nano-plastics

Article

Uptake and Cellular Effects of Polymethylmethacrylate on Human Cell Lines

Arthur Braun and Harald Seitz *

Fraunhofer Institute for Cell Therapy and Immunology, Branch Bioanalytics and Bioprocesses, 14476 Potsdam, Germany

* Correspondence: harald.seitz@izi-bb.fraunhofer.de; Tel.: +49 331 58187-208

Abstract: Both the use of plastic and its decomposition products lead to the distribution of plastic all over the earth and finally to the uptake by all kind of living beings including humans. Still, it is widely unknown what risks harbor the widespread uptake of plastics for human health, especially regarding contributing factors like size, shape and surface composition. We assessed the uptake of polymethylmethacrylate (PMMA)-nano- and microbeads for HEK293-, A549- and MRC5 cells. Via confocal microscopy, we localized multiple PMMA-beads inside the cytosol of cells. Uptake of PMMA-beads did not alter cell growth and cell division, implying no short-term toxicity towards human cells. Further, we used a cAMP response element binding protein (CREB)-mediated reporter assay to assess whether internalized PMMA-nanobeads alter cell-signaling pathways. In contrast to the *in vitro* transcription, where the addition of PMMA-nanobeads abolished the transcription, no changes regarding CREB-mediated cell signaling are given in HEK293-cells. Our data led to the assumption that PMMA-nano-and microbeads are internalized via endocytosis and end up as lysosomes within the cells cytosol. Therefore, we concluded differences regarding the surface composition of the PMMA-nanobeads mainly affect its potential to alter cell signaling. These findings emphasize the key role the surface composition plays regarding microplastic and its risks for human health.

Keywords: CREB; PMMA; micro-plastics; confocal microscopy; nano-plastics

1. Introduction

Despite all efforts to reduce plastic use and increase recycling, the amount of plastic produced annually increases [1]. Both the decay of waste as well as the intentional usage of microplastics (< 5 mm) led to an ubiquitous distribution around the world [2–4]. Microplastics are present in drinking water, air and food. Furthermore, microplastic can act as a vector for harmful chemicals and pathogens, imposing additional threats to human health [5]. Upon uptake, microplastics induce inflammation, neurotoxicity, oxidative stress and changes in the metabolome in eukaryotic organisms [3,6,7]. Polymethylmethacrylate (PMMA) is a synthetic polymer used in the medical area as "bone cement" for implant fixation [8]. Additionally various drug delivery systems based on PMMA-nanobeads have been and are currently researched with a variety of applications [9–11]. The usage of PMMA mainly derives from its biocompatibility, robustness and low toxicity [12]. With it being a beneficial material for the medical area, questions arise whether its use as a drug delivery system as well as the unintentional uptake of PMMA harbors risks for humans [13]. Studies already proved that humans ingest nano- and microplastics from various sources resulting in an accumulation within the lungs, kidney and liver [14]. Recently it was also shown that, after ingestion, microplastics are detected in the human urine. This means that these particles are adsorbed via the digestive tract or pulmonary diffusion and excreted via the kidney [15]. For that reason, lungs, kidneys and liver are especially prone to harmful effects after ingestion. We used confocal imaging techniques to investigate if PMMA nano- and microbeads are internalized by HEK293, A549 or MRC5 cells or remain at the surface of cells. Furthermore, we analyzed the influence of PMMA-beads on signal transduction pathways. With the addition of PMMA resulting in an abolished cAMP response element binding protein (CREB) mediated *in vitro* transcription, altered CREB signaling after uptake of PMMA by human cells is expected [16]. CREB is ubiquitously expressed and part of various

 doi:10.20944/preprints202311.1844.v1

eukaryotic signaling processes, especially in the development of long-term memories [17]. Disturbances regarding CREB signaling can result in defect neuronal development, hematopoiesis and play a role in the emerging of cognitive and neurodegenerative disorders [18,19]. The aim of this study was to visualize the uptake of PMMA by human cells and to investigate whether the incubation of HEK293 cells with PMMA cells will alter CREB signaling.

2. Materials and Methods

Cell Culture

HEK293 and A549 cells (DSMZ, Braunschweig, Germany) were cultivated in DMEM (Sigma-Aldrich, Taufkirchen, Germany) while MRC5 cells (ATCC, Manassas, VA, USA) were cultivated in Alpha-MEM (Biowest, Nuaillé, France) with 10 % fetal bovine serum added (Biowest, Nuaillé, France) at 37 °C, 5 % CO_2. Every two to three days cells were passaged to not exceed 80 % confluency. Doubling times were determined to assess whether PMMA-beads reduce cell growth and division. Using a 24 well plate, $5*10^4$ cells per well were incubated with different amounts of PMMA-beads for 72 h. After incubation cell nuclei were stained for 20 minutes with a phosphate buffered saline (PBS) solution containing 5 µg/mL Hoechst 33342 (Abcam, Cambridge, Great Britain). Images were acquired using the IX83 from Olympus (Tokyo, Japan), whereby the microscope software "scanR" enables cell counting using the pictures acquired after staining the cell nuclei. Using this equation, the doubling time (t_D) was calculated:

$$t_D = \frac{\log_{10}(2) * incubation\ time\ [h]}{\log_{10} N - \log_{10} N_0}$$

with N_0 being the number of cells at the start and N after 72 hours.

Confocal imaging

For confocal imaging HEK293, A549 and MRC5 cells were seeded out in an eight well chambered coverslip (ibidi, Gräfelfing, Germany) with each well containing $2*10^4$ cells and $4.5*10^9$ beads/mL. After incubation for 48 hours cells were fixed with 4 % (m/v) paraformaldehyde for 15 minutes, washed two times with PBS and then stained for 30 minutes using a PBS solution containing 5 µg/mL Hoechst 33342 and 200 µg/mL Concanavalin A (Con A)-Alexa Fluor™ 594 (ThermoFisher, Hennigsdorf, Germany). Hoechst 33342 is a fluorescent dye used to stain the nucleus while Con A binds to carbohydrates, mainly found on the cell membrane. Images were collected using a LSM 710 from Zeiss (Jena, Germany) with 40x/63x magnification. Image analysis was performed via ImageJ 1.54b software.

Transfection

HEK293 cells were plated at a density of $3*10^4$ /24 well with PMMA-nanobeads ($4.5*10^9$ beads/mL) and after 72 h transfected with the following plasmids: CMV-MGFP as the positive control, CRE-MGFP as the inducible gene and TATA-MGFP linked to a non-inducible region as the negative control [16]. All three plasmids are part of a Cignal Reporter Assay Kit (Qiagen, Venlo, Netherlands) and based on the stimulation of a CREB-mediated protein kinase A (PKA) signaling pathway. Prior to stimulation, cells are washed twice with PBS 24 h after transfection and incubated with DMEM absent of fetal calf serum for 2 hours. For stimulation 50 µM forskolin (Merck, Darmstadt, Germany) and 50 µM 3-Isobutyl-1-methylxanthin (IBMX, Merck, Darmstadt, Germany) are then added. After 4 h of incubation, the resulting fluorescence is measured each hour for a 4 h period using an IX83 from Olympus (Tokyo, Japan). The resulting intensity profiles were analyzed using ImageJ 1.54b software.

 doi:10.20944/preprints202311.1844.v1

Image Analysis

For each fluorophore present during confocal imaging, an own color channel image was acquired showing the excitation of either Hoechst 33342, Con A-Alexa Fluor™ 594 or the PMMA-beads. The three channels are then merged via ImageJ. To analyze the intensity profiles after the stimulation of transfected HEK293 cells (see *Transfection*) with and without PMMA a binary image is created which contains the intensity for each cell emitting light after excitation of MGFP. For each cell present in the image acquired, ImageJ will determine the average intensity. The cutoff value of the pixel intensity to differentiate between background and cells is 5000. All objects smaller than 90 μm^2 are excluded from the evaluation. This allows sufficient differentiation between cells and background artefacts. By plotting the intensity for each hour after stimulation, intensity profiles are generated showing the course of the intensity distribution within all cells detected.

Statistics

Data are presented as means ± SEM. N being defined as number of biological replicates with the exact number of biological replicates shown at each section. Data evaluation was performed using RStudio 2023.09.1 (Posit PBS, Boston, MA, USA).

Beads

Fluorescent PMMA-beads were purchased from PolyAn (Berlin, Germany). The fluorophore "PolyAn Orange" is incorporated into the PMMA matrix during polymerization, preventing leak-out. The beads are covered with carboxy groups enabling coupling of proteins. Nanobeads with 165 nm diameter and microbeads with 2 µm diameter were used in this study.

3. Results

Confocal imaging

Due to the accumulation of microplastic in lungs and kidneys, cells embodied in those organs are exposed to effects from the uptake of microplastic [20]. As previous literature indicates HEK293 and A549 cells uptake PMMA whereas for MRC5 no literature regarding the uptake of PMMA is found [21,22]. By visualizing whether PMMA-beads enter the cytosol of the three cell lines, presumptions can be made whether it is likely that PMMA will have an effect on signal transduction pathways of human cell lines.

Con A was used to stain the cell membrane allowing the visualization of the interface between outside and inside of the cell. We were able to detect PMMA-beads inside the cytosol of HEK293, A549 and MRC5-cells. For each cell line, multiple beads entered the cell. The beads were randomly distributed within the cytosol. No PMMA-beads were detected within the nucleus. Beads appear rather yellow than green, indicating a membrane surrounding the beads and therefore allowing the binding of Con A to the beads. The size of the beads was determined using ImageJ and is shown in Table 1. Due to aggregation the determined size of the nanobeads (~0.6 µm) differs by a factor of 3 from the starting material (Ø = 165 nm). We cannot discriminate exactly at which point the aggregation occurred. PMMA-beads incubated with DMEM in the absence of cells showed aggregation already, indicating that the aggregation likely took place before the uptake by cells. The microbeads showed no aggregation, with size measurements averaging at 2.03 µm.

Table 1. Average size of green objects seen in Figure 1.

Figure	**(a)**	**(b)**	**(c)**	**(d)**
Cell line	HEK293	HEK293	A549	MRC5
Average size (µm) determined	0.54 ± 0.29	2.03 ± 0.19	0.76 ± 0.27	0,66 ± 0,47
Average size (µm) of the beads	0.165	2	0.165	0.165
Polydispersity Index	9,1 %	8,9 %	9,1 %	9,1 %

 doi:10.20944/preprints202311.1844.v1

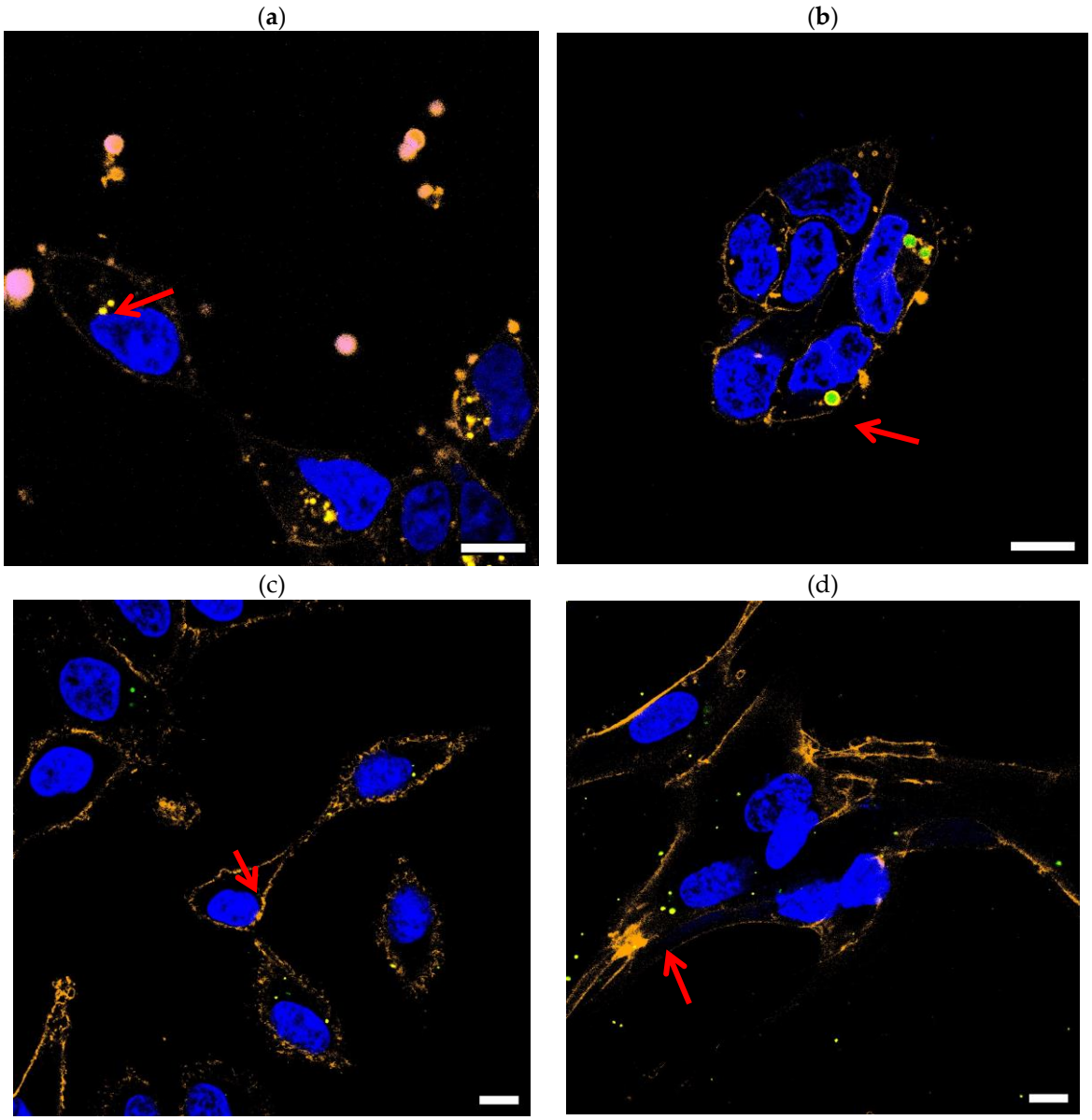

Figure 1. Confocal images showing HEK293 (a, b), A549 (c) and MRC5 (d) cells after incubation for 48 h with polymethylmethacrylate (PMMA)-beads (green). Concanavalin A (Con A)-Alexa Fluor™ 594 (orange) was used to visualize the cell membrane while Hoechst 33342 was used as a nuclear stain (blue). In (a), (c) and (d) cells were incubated with PMMA-nanobeads (Ø = 165 nm). In (b) cells were incubated with PMMA-microbeads (Ø = 2 µm). Red arrows indicate the position of PMMA. Scale bars represent 10 µm.

Doubling time

Cells were incubated with varying amounts of PMMA for 72 hours. After incubation cells were stained with Hoechst 33342. Using the fluorescence microscope IX83 images were acquired of the cells. ScanR, a processing software, allows the determination of the number of cells after 72 h of incubation, allowing the calculation of the doubling time t_D. Results are summarized in Table 2.

 doi:10.20944/preprints202311.1844.v1

Table 2. Doubling time of HEK293, A549 and MRC5 cells after incubation with PMMA for 72 h (n=3).

cell line	Ø	Beads/mL	t_D (h)
HEK293	165 nm	$4.5*10^9$	26.00 ± 3.85
		$4.5*10^8$	25.96 ± 3.49
		0	27.44 ± 2.33
	2 µm	$2.53*10^6$	28.84 ± 2.95
		$2.53*10^5$	29.94 ± 3.01
		0	29.56 ± 2.75
A549	165 nm	$4.5*10^9$	30.84 ± 1.64
		$4.5*10^8$	33.17 ± 3.89
		0	29.86 ± 1.62
	2 µm	$2.53*10^6$	29.21 ± 1.36
		$2.53*10^5$	28.61 ± 3.30
		0	29.44 ± 2.76
MRC5	165 nm	$4.5*10^9$	51.26 ± 7.91
		$4.5*10^8$	46.30 ± 4.66
		0	45.44 ± 4.37
	2 µm	$2.53*10^6$	45.16 ± 7.56
		$2.53*10^5$	47.48 ± 9.07
		0	46.25 ± 7.32

The doubling times of HEK293, A549 and MRC5 cells incubated without PMMA-nano- and microbeads are in line with those found in other publications [23–25]. Only at excessively high particle densities, a significant deviation of the doubling time was measured. Cells did not adhere to the growth surface and remained circular in suspension, indicating cell apoptosis. Apart from that, incubation with PMMA resulted in no significant reduction of cell growth, cell division and alteration in cell morphology. This indicates that PMMA shows no short-term toxicity towards the growth and division of HEK293-, A549- and MRC5-cells.

Transfection

The plasmids used for transfection derive from a reporter assay kit used for quantitative assessment of signal transduction pathways. Previously it has been shown that the addition of PMMA-nanobeads will result in an abolished *in vitro* gene expression [16]. Transfection using the same plasmids enables assessment whether CREB-mediated signaling is altered in HEK293 cells due to the presence of PMMA as well. The resulting intensity after stimulation is shown in Figure 2. HEK293-cells were transfected with CMV-MGFP as the positive control, CRE-MGFP as the reporter construct and TATA-MGFP linked to a non-inducible region as the negative control. Prior to transfection and stimulation cells were incubated with PMMA-nanobeads (Ø = 165 nm, $4.5*10^9$ beads /mL) or PBS for 72 h.

Incubation with PMMA-nanobeads ($4.5*10^9$ beads /mL) did not alter CREB-mediated cell signaling. For CMV-MGFP (positive control), prior incubation with PBS results in an average intensity of 10451±3401 after 4 h with no significant changes over the course of the experiment. Incubation with PMMA-nanobeads results in a similar initial intensity with 10191±3787 while also no significant changes are given over time. Stimulation of transfected HEK293-cells with the CRE-MGFP (reporter) shows an increase of the intensity measured over time independently of prior incubation with PBS or PMMA-nanobeads. The average intensity for incubation with PBS rises from 7042±1605 to 13136±6044, showing a clear stimulation of the signaling pathway. Similarly, the intensity rises for prior incubation with PMMA from 7124±1350 to 13096±5867. The data shows CREB-mediated cell signaling through stimulation using forskolin and IBMX is not altered by prior incubation with PMMA-nanobeads.

 doi:10.20944/preprints202311.1844.v1

(**a**) CMV-MGFP, PBS (**b**) CMV-MGFP, PMMA-NB 4.5*10^9 beads/mL

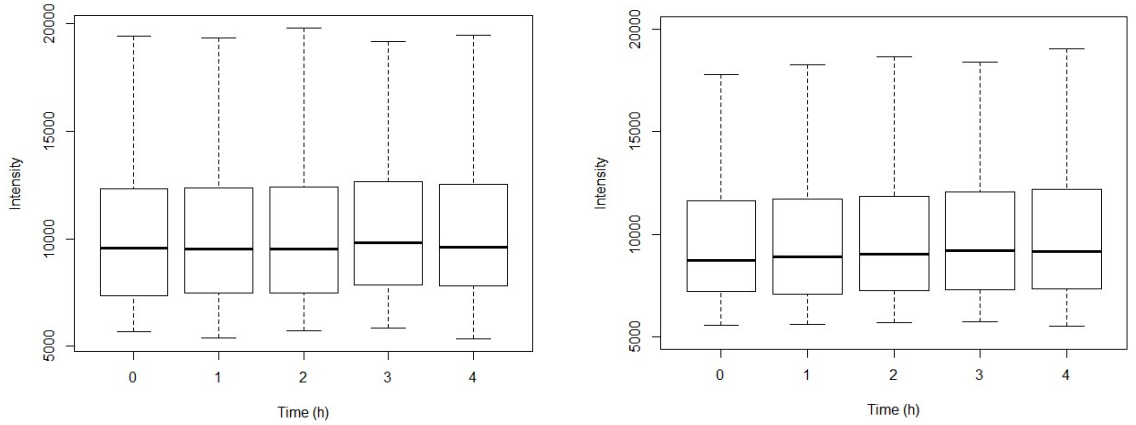

(c) CRE-MGFP, PBS (d) CRE-MGFP, PMMA-NB 4.5*10^9 beads /mL

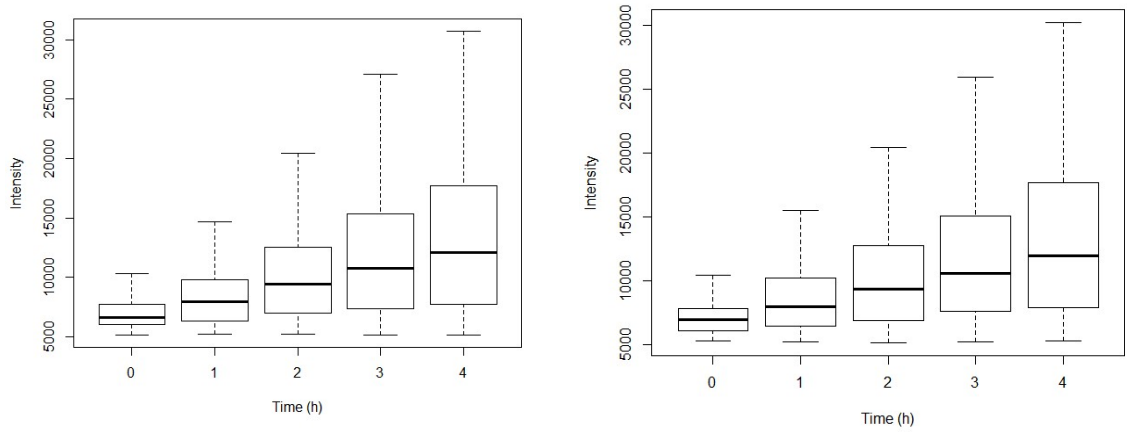

Figure 2. Quantification of cAMP response element binding protein (CREB)-mediated signaling in HEK293-cells after stimulation with forskolin and 3-Isobutyl-1-methylxanthin (IBMX). Prior to stimulation cells in (a) and (b) were incubated with whether PBS or PMMA-nanobeads and then transfected with CMV-MGFP (positive control). Cells in (c) and (d) were also incubated with whether PBS or PMMA-nanobeads but then transfected using the CRE-MGFP (reporter).

4. Discussion

Confocal Imaging

Since the surface of human cells is covered with glycoproteins and glycolipids, staining with fluorophore-coupled Con A allows visualization of the cell membrane via fluorescence microscopy. This allows the determination whether PMMA-beads are within cells or outside, as the cell membrane serves as an interface between. HEK293-, A549- and MRC5-cells uptake PMMA [21,22]. The images in Figure 1 show multiple beads located within HEK293-, A549- and MRC5-cells. PMMA-beads were randomly distributed within the cytosol of the cells. Previous reports suggest the uptake of PMMA-beads is via endocytosis. During this process, the beads end up as late endosomes and lysosomes [26]. Lysosomes are embedded within a membrane containing glycoproteins on its surface, hence the binding of Con A is observed [27]. This results in the mixing of fluorescence signals with beads appearing yellow rather than green. The size of internalized PMMA-nanobeads increases by a factor of 3. This indicates an aggregation occurring within the PMMA-nanobeads. In a complex environment like biological media, nanoparticles tend to aggregate [28]. The observed aggregation of the beads most likely takes place before the uptake by cells. During uptake, these aggregates

 doi:10.20944/preprints202311.1844.v1

remain intact and enter the cytosol. Coincidentally the size of the nanobead-aggregates is within the usual size of lysosomes, ranging between 200 and 600 nm, further supporting that the mechanism behind the uptake of PMMA-beads is endocytosis [29]. Regarding PMMA microbeads (2 µm), no aggregation was observed after incubation with cells. The aggregation of nanobeads can be of relevance regarding drug delivery systems based on PMMA-nanobeads, especially since aggregation of intravenously administered nano-therapeutics result in an increased clearance in the liver [28]. Due to the fixation of cells necessary for fluorescence staining, quantification of PMMA-beads per cell was not possible in this experimental setup. Nonetheless, a dependency is detectable regarding the uptake of PMMA-beads by HEK293-, A549- and MRC5-cells. The larger the diameter of the beads, the smaller the number of beads taken up by each cell.

Doubling time

In accordance with other publications, the incubation of HEK293 and A549 cells with PMMA-beads resulted in no significant reduction of cells counted, with the doubling times remaining unaffected. No major effects of PMMA on cell growth, division and cell cycle are given [21,30,31]. No publication is found regarding the cytotoxicity of PMMA towards MRC5. Our results indicate no major effects are given, due to the doubling times not being altered by incubation with PMMA as well. Beads are split evenly between cells with the distribution of the beads appearing random during cell division. Only by incubation with excessively high amounts of PMMA a reduction of cell growth can be seen. While the uptake of excessive amounts of PMMA by a human is unlikely, due to the local enrichment of microplastics in human organisms, local harmful effects cannot be excluded entirely. Since we only investigated the direct exposure of PMMA-beads human cell lines, no assumptions can be made regarding long-term toxicity.

Transfection

The addition of 100 µg/mL PMMA-nanobeads abolishes the CREB-mediated *in vitro* transcription using the same reporter assay as in this work [16]. With HEK293-cells able to internalize PMMA-nanobeads, we expected similar effects within the cells. Regarding cells transfected with the CMV-MGFP plasmid, the constitutive expression of MGFP is not altered. Since nanobeads are not entering the cell nucleus after internalization, no inhibition of transcription can occur. Nevertheless, internalized microplastics can alter cellular structures and interact with proteins resulting in conformational changes of the protein secondary structure and loss of function [32]. This is heavily influenced by the surface composition of the microplastic though, influencing it's biological fate and toxicity [33]. Aggregation and uptake of PMMA-beads via endocytosis results in the beads being embedded in a membrane. Due to this, no alteration regarding the translation of MGFP within the cytosol is given after uptake by HEK293-cells as well. Furthermore, transfection of HEK293-cells with the CRE-MGFP plasmid and stimulation of PKA signaling pathways via forskolin and IBMX are not altered by the presence of PMMA-nanobeads within the cytosol as well. The resulting expression of MGFP remains unaffected when comparing that of cells prior incubated with PBS to cells incubated with PMMA-nanobeads. These results underline the role the surface composition plays regarding the toxicity of microplastics in general. While the *in vitro* transcription can be abolished by adding PMMA-beads, no equivalent alteration is given within HEK293-cells. This implies that after the uptake by HEK293-cells, the PMMA nanobeads lose the ability to alter cell signaling via loss of function for essential proteins.

Microplastic in land and sea is continuously in contact with a complex biological environment exposed to constant physical and chemical changes. For risk assessment regarding human health the relationship between the biological environment, chemical degradation and aging resulting in changes regarding the surface composition of microplastics need to be determined. Understanding the role the surface composition plays is key for a better understanding of the toxicity of internalized microplastics.

Author Contributions: Arthur Braun and Harald Seitz designed the experiments. Arthur Braun performed the experiments. Arthur Braun wrote the paper together with Harald Seitz. All authors discussed the results and commented on the manuscript. All authors have read and agreed to the published version of the manuscript.

Funding: This research received no external funding.

Institutional Review Board Statement: Not applicable

Informed Consent Statement: Not applicable

Data Availability Statement: The data presented in this study are available on request from the corresponding author.

Acknowledgments: We would like to thank Professor Ralph Gräf from the University of Potsdam for allowing the usage of the confocal microscope.

Conflicts of Interest: The authors declare no conflict of interest.

References

1. Geyer, R.; Jambeck, J.R.; Law, K.L. Production, Use, and Fate of All Plastics Ever Made. *Sci. Adv.* **2017**, *3*, e1700782, doi:10.1126/sciadv.1700782.
2. Moore, C.J. Synthetic Polymers in the Marine Environment: A Rapidly Increasing, Long-Term Threat. *Environ. Res.* **2008**, *108*, 131–139, doi:10.1016/j.envres.2008.07.025.
3. Hidalgo-Ruz, V.; Gutow, L.; Thompson, R.C.; Thiel, M. Microplastics in the Marine Environment: A Review of the Methods Used for Identification and Quantification. *Environ. Sci. Technol.* **2012**, *46*, 3060–3075, doi:10.1021/es2031505.
4. Yokota, K.; Waterfield, H.; Hastings, C.; Davidson, E.; Kwietniewski, E.; Wells, B. Finding the Missing Piece of the Aquatic Plastic Pollution Puzzle: Interaction between Primary Producers and Microplastics. *Limnol. Oceanogr. Lett.* **2017**, *2*, 91–104, doi:10.1002/lol2.10040.
5. Caruso, G. Microplastics as Vectors of Contaminants. *Mar. Pollut. Bull.* **2019**, *146*, 921–924, doi:10.1016/j.marpolbul.2019.07.052.
6. Xiang, C.; Chen, H.; Liu, X.; Dang, Y.; Li, X.; Yu, Y.; Li, B.; Li, X.; Sun, Y.; Ding, P.; et al. UV-Aged Microplastics Induces Neurotoxicity by Affecting the Neurotransmission in Larval Zebrafish. *Chemosphere* **2023**, *324*, 138252, doi:10.1016/j.chemosphere.2023.138252.
7. Qiao, R.; Sheng, C.; Lu, Y.; Zhang, Y.; Ren, H.; Lemos, B. Microplastics Induce Intestinal Inflammation, Oxidative Stress, and Disorders of Metabolome and Microbiome in Zebrafish. *Sci. Total Environ.* **2019**, *662*, 246–253, doi:10.1016/j.scitotenv.2019.01.245.
8. Vaishya, R.; Chauhan, M.; Vaish, A. Bone Cement. *J. Clin. Orthop. Trauma* **2013**, *4*, 157–163, doi:10.1016/j.jcot.2013.11.005.
9. Gad, M.; Fouda, S.; Al-Harbi, F.; Näpänkangas, R.; Raustia, A. PMMA Denture Base Material Enhancement: A Review of Fiber, Filler, and Nanofiller Addition. *Int. J. Nanomedicine* **2017**, *Volume 12*, 3801–3812, doi:10.2147/IJN.S130722.
10. Lin, M.; Wang, H.; Meng, S.; Zhong, W.; Li, Z.; Cai, R.; Chen, Z.; Zhou, X.; Du, Q. Structure and Release Behavior of PMMA/Silica Composite Drug Delivery System. *J. Pharm. Sci.* **2007**, *96*, 1518–1526, doi:10.1002/jps.20809.
11. Prabakaran, S.; Jeyaraj, M.; Nagaraj, A.; Sadasivuni, K.K.; Rajan, M. Polymethyl Methacrylate–Ovalbumin @ Graphene Oxide Drug Carrier System for High Anti-Proliferative Cancer Drug Delivery. *Appl. Nanosci.* **2019**, *9*, 1487–1500, doi:10.1007/s13204-019-00950-5.
12. Tihan, T.G.; Ionita, M.D.; Popescu, R.G.; Iordachescu, D. Effect of Hydrophilic–Hydrophobic Balance on Biocompatibility of Poly(Methyl Methacrylate) (PMMA)–Hydroxyapatite (HA) Composites. *Mater. Chem. Phys.* **2009**, *118*, 265–269, doi:10.1016/j.matchemphys.2009.03.019.
13. De Jong, W.H.; Borm, P.J. Drug Delivery and Nanoparticles: Applications and Hazards. *Int. J. Nanomedicine* **2008**, *3*, 133–149, doi:10.2147/ijn.s596.
14. Yang, Y.-F.; Chen, C.-Y.; Lu, T.-H.; Liao, C.-M. Toxicity-Based Toxicokinetic/Toxicodynamic Assessment for Bioaccumulation of Polystyrene Microplastics in Mice. *J. Hazard. Mater.* **2019**, *366*, 703–713, doi:10.1016/j.jhazmat.2018.12.048.
15. Pironti, C.; Notarstefano, V.; Ricciardi, M.; Motta, O.; Giorgini, E.; Montano, L. First Evidence of Microplastics in Human Urine, a Preliminary Study of Intake in the Human Body. *Toxics* **2022**, *11*, 40, doi:10.3390/toxics11010040.
16. Pellegrino, A.; Danne, D.; Weigel, C.; Seitz, H. An In Vitro Assay to Quantify Effects of Micro- and Nano-Plastics on Human Gene Transcription. *Microplastics* **2023**, *2*, 122–131, doi:10.3390/microplastics2010009.
17. Kida, S.; Serita, T. Functional Roles of CREB as a Positive Regulator in the Formation and Enhancement of Memory. *Brain Res. Bull.* **2014**, *105*, 17–24, doi:10.1016/j.brainresbull.2014.04.011.

18. Oike, Y.; Takakura, N.; Hata, A.; Kaname, T.; Akizuki, M.; Yamaguchi, Y.; Yasue, H.; Araki, K.; Yamamura, K.; Suda, T. Mice Homozygous for a Truncated Form of CREB-Binding Protein Exhibit Defects in Hematopoiesis and Vasculo-Angiogenesis. *Blood* **1999**, *93*, 2771–2779, doi:10.1182/blood.V93.9.2771.
19. Saura, C.A.; Valero, J. The Role of CREB Signaling in Alzheimer's Disease and Other Cognitive Disorders. *revneuro* **2011**, *22*, 153–169, doi:10.1515/rns.2011.018.
20. Pitt, J.A.; Kozal, J.S.; Jayasundara, N.; Massarsky, A.; Trevisan, R.; Geitner, N.; Wiesner, M.; Levin, E.D.; Di Giulio, R.T. Uptake, Tissue Distribution, and Toxicity of Polystyrene Nanoparticles in Developing Zebrafish (Danio Rerio). *Aquat. Toxicol.* **2018**, *194*, 185–194, doi:10.1016/j.aquatox.2017.11.017.
21. Da Silva Brito, W.A.; Singer, D.; Miebach, L.; Saadati, F.; Wende, K.; Schmidt, A.; Bekeschus, S. Comprehensive in Vitro Polymer Type, Concentration, and Size Correlation Analysis to Microplastic Toxicity and Inflammation. *Sci. Total Environ.* **2023**, *854*, 158731, doi:10.1016/j.scitotenv.2022.158731.
22. Adinolfi, B.; Pellegrino, M.; Tombelli, S.; Trono, C.; Giannetti, A.; Domenici, C.; Varchi, G.; Sotgiu, G.; Ballestri, M.; Baldini, F. Polymeric Nanoparticles Promote Endocytosis of a Survivin Molecular Beacon: Localization and Fate of Nanoparticles and Beacon in Human A549 Cells. *Life Sci.* **2018**, *215*, 106–112, doi:10.1016/j.lfs.2018.11.007.
23. Jacobs, J.P.; Jones, C.M.; Baille, J.P. Characteristics of a Human Diploid Cell Designated MRC-5. *Nature* **1970**, *227*, 168–170, doi:10.1038/227168a0.
24. Russell, W.C.; Graham, F.L.; Smiley, J.; Nairn, R. Characteristics of a Human Cell Line Transformed by DNA from Human Adenovirus Type 5. *J. Gen. Virol.* **1977**, *36*, 59–72, doi:10.1099/0022-1317-36-1-59.
25. Assanga, I. Cell Growth Curves for Different Cell Lines and Their Relationship with Biological Activities. *Int. J. Biotechnol. Mol. Biol. Res.* **2013**, *4*, 60–70, doi:10.5897/IJBMBR2013.0154.
26. Vollrath, A.; Schallon, A.; Pietsch, C.; Schubert, S.; Nomoto, T.; Matsumoto, Y.; Kataoka, K.; Schubert, U.S. A Toolbox of Differently Sized and Labeled PMMA Nanoparticles for Cellular Uptake Investigations. *Soft Matter* **2013**, *9*, 99–108, doi:10.1039/C2SM26928G.
27. Saftig, P.; Klumperman, J. Lysosome Biogenesis and Lysosomal Membrane Proteins: Trafficking Meets Function. *Nat. Rev. Mol. Cell Biol.* **2009**, *10*, 623–635, doi:10.1038/nrm2745.
28. Moore, T.L.; Rodriguez-Lorenzo, L.; Hirsch, V.; Balog, S.; Urban, D.; Jud, C.; Rothen-Rutishauser, B.; Lattuada, M.; Petri-Fink, A. Nanoparticle Colloidal Stability in Cell Culture Media and Impact on Cellular Interactions. *Chem. Soc. Rev.* **2015**, *44*, 6287–6305, doi:10.1039/C4CS00487F.
29. Barral, D.C.; Staiano, L.; Guimas Almeida, C.; Cutler, D.F.; Eden, E.R.; Futter, C.E.; Galione, A.; Marques, A.R.A.; Medina, D.L.; Napolitano, G.; et al. Current Methods to Analyze Lysosome Morphology, Positioning, Motility and Function. *Traffic* **2022**, *23*, 238–269, doi:10.1111/tra.12839.
30. Khan, F.A.; Akhtar, S.; Almohazey, D.; Alomari, M.; Almofty, S.A.; Badr, I.; Elaissari, A. Targeted Delivery of Poly (Methyl Methacrylate) Particles in Colon Cancer Cells Selectively Attenuates Cancer Cell Proliferation. *Artif. Cells Nanomedicine Biotechnol.* **2019**, *47*, 1533–1542, doi:10.1080/21691401.2019.1577886.
31. Feuser, P.E.; Gaspar, P.C.; Ricci-Júnior, E.; Silva, M.C.S.D.; Nele, M.; Sayer, C.; H. H. De Araújo, Pedro. Synthesis and Characterization of Poly(Methyl Methacrylate) PMMA and Evaluation of Cytotoxicity for Biomedical Application. *Macromol. Symp.* **2014**, *343*, 65–69, doi:10.1002/masy.201300194.
32. Windheim, J.; Colombo, L.; Battajni, N.C.; Russo, L.; Cagnotto, A.; Diomede, L.; Bigini, P.; Vismara, E.; Fiumara, F.; Gabbrielli, S.; et al. Micro- and Nanoplastics' Effects on Protein Folding and Amyloidosis. *Int. J. Mol. Sci.* **2022**, *23*, 10329, doi:10.3390/ijms231810329.
33. Wang, J.; Cong, J.; Wu, J.; Chen, Y.; Fan, H.; Wang, X.; Duan, Z.; Wang, L. Nanoplastic-Protein Corona Interactions and Their Biological Effects: A Review of Recent Advances and Trends. *TrAC Trends Anal. Chem.* **2023**, *166*, 117206, doi:10.1016/j.trac.2023.117206.